Blöcher, G., Zimmermann, G., Milsch, H. (2009): Impact of poroelastic response of sandstones on geothermal power production. - Pure and Applied Geophysics, 166, 5-7, 1089-1106

DOI: 10.1007/s00024-009-0475-4.

Impact of poroelastic response of sandstones on geothermal power production

M. G. Blöcher, G. Zimmermann & H. Milsch

GeoForschungsZentrum Potsdam, Telegrafenberg, D-14473 Potsdam, Germany

Potsdam, March 19, 2009

Abstract

During geothermal power production using a borehole doublet consisting of a production and injection well, the reservoir conditions such as permeability k, porosity ϕ and Skempton coefficient B at the geothermal research site Gross Schönebeck/Germany will change. Besides a temperature decrease at the injection well and a change of the chemical equilibrium, also the pore pressure p_p will vary in a range of approximately 44 MPa ± 10 MPa in our reservoir at -3850 to -4258 m depth. This leads to a poroelastic response of the reservoir rocks depending on effective pressure p_{eff} (difference between mean stress and pore pressure), resulting in a change in permeability k, porosity ϕ and the poroelastic parameter Skempton coefficient B. Hence, we investigated the effective pressure dependency of Flechtinger sandstone, an outcropping equivalent of the reservoir rock via laboratory experiments. The permeability decreased by 21% at an effective pressure range from 3 to 30 MPa, the porosity decreased by 11% (p_{eff} = 6 to 65 MPa) and the Skempton coefficient decreased by 24% (p_{eff} = 4 to 25 MPa). We will show, which mechanisms lead to the change of the mentioned hydraulic and poroelastic parameters and the influence of these changes on the productivity of the reservoir. The most significant changes occur at low effective pressures until 15 to 20 MPa. For our in situ reservoir conditions $p_{eff} = 43MPa$ a change of 10 MPa effective pressure will result in a change in matrix permeability of less than 4% and in matrix porosity of less than 2%. Besides natural fracture systems, fault zones and induced hydraulic fractures, the rock matrix its only one part of geothermal systems. All components can be influenced by pressure, temperature and chemical reactions. Therefore, the determined small poroelastic response of rock matrix does not significantly influence the sustainability of the geothermal reservoir.

Introduction

The technical feasibility of geothermal power production will be demonstrated by means of the geothermal research wells Gross Schoenebeck (40 km north of Berlin/Germany) using a borehole doublet. The reservoir is located in -3850 to -4258 m depth within the Lower Permian of the NE German Basin. The main targets are sandstones of the Upper Rotliegend (Dethlingen Formation/lower Elbe subgroup) as well as the volcanic rocks (andesites) of the Lower Rotliegend, where permeability is mainly due to connected fractures. The Dethlingen sandstones represent an effective reservoir horizon with a porosity of 8-10% and a permeability of $1 * 10^{-14}$ to $1 * 10^{-13} m^2$ (TRAUTWEIN and HUENGES, 2005). During geothermal power production using the doublet for production and injection simultaneously flow rates up to 100 m^3/h will be applied (ZIMMERMANN et al., 2008). According to the productivity index $PI = 10 m^3/(h * MPa)$ (ZIMMERMANN and REINICKE, 2008), which is defined as the ratio between flow rate and pore pressure change in the reservoir during water production, a pore pressure change dp_p of $\pm 10 MPa$ will be induced. The in situ formation pressure is $p_p = 43.8 MPa$, determined by p,T-logs at stationary conditions of the geothermal target horizon at a depth of 4100 m (LEGARTH et al., 2005). In addition to a fault pattern analysis, stress ratios were calculated for the -4035 m deep Rotliegend sediments based on frictional failure theory (MOECK et al., 2008). By means of the stress ratios and the vertical stress S_V =105 MPa the maximum horizontal stress S_H = 100 MPa and the minimum horizontal stress S_h = 55MPa were determined. By means of the mean stress $\bar{\sigma} = (S_V + S_H + S_h)/3 = 82.7 MPa$ the effective mean stress $\bar{\sigma}_{eff} = \bar{\sigma} - p_p = 42.9 MPa$ can be calculated (TERZAGHI, 1923). For our particular case an effective stress range of $42.9 \pm 10 MPa$ is of interest.

In order to show the influence of this effective stress change on the geothermal power production, we investigated the effective pressure dependency of the hydraulic rock properties permeability k and porosity ϕ as well as the hydro-mechanical property Skempton coefficient B (SKEMPTON, 1954). The permeability is a measure of the ability of the reservoir rock to conduct water and therefore influences the potential production rate. The porosity indicates the potential volume of geothermal fluid in the reservoir rock and the Skempton coefficient indicates the mechanical reservoir behavior on pore pressure change. The investigation was done by means of laboratory experiments with Flechtinger sandstone (Sventesius quarry, Germany), an outcropping equivalent of the reservoir rock.

Various previous studies still investigated the effective pressure dependency of these rock properties. CARROLL and KATSUBE (1983) developed a theory of hydrostatic poroelasticity in terms of porosity and bulk volume. By means of this theory changes in effective pressure can related to changes in porosity (ZIMMERMAN, 1991). The effective stress dependency of the porosity also controls changes of elastic moduli and the seismic velocity (SHAPIRO, 2003). The permeability can always be expressed as a function of confining p_c and pore pressure p_p (AL-WARDY and ZIMMERMAN, 2003). If the permeability follows the effective pressure law $p_{eff} = p_c - \chi p_p$, where χ denotes the effective pressure coefficient, then it can be expressed as a function of this effective pressure, $k = f(p_c - \chi p_p)$. Several experiments determined the effective pressure coefficient χ; MORROW et al. (1986) and BERNABE (1987) found that a value of 1 was the limiting value for crystalline rocks, ZOBACK and BYERLEE (1975) and AL-WARDY and ZIMMERMAN (2003) found that the effective stress coefficient depends on the clay content. Often χ is taken to be constant, yielding a linear expression for effective pressure, but KWON et al. (2001, and references therein) mentioned that χ may itself be a function of pressures p_c or p_p, or microstructural changes in pore structure.

The dependency of permeability on pore structure was also investigated by various studies: A general overview can be found in BEAR (1972); using hydraulic radius models (KOZENY, 1927; CARMAN, 1937) or geometric parameters determined by a fractal approach (PAPE et al., 2000) or mercury injection (KATZ and THOMPSON, 1987). It has to be taken into account, that the pore geometry parameters cannot be directly measured under pressure. Therefore, the permeability has to be correlated to other rock properties such as porosity or formation factor (BERNABE, 1988), which can be measured under pressure. Besides permeability also the Skempton coefficient was investigated under different experimental conditions. These studies showed that B is nearly independent of deviatoric stress change, but decreases as a result of the stiffening effect due to increasing confining pressure (LOCKNER and STANCHITS, 2002), under axisymmetric loading (LOCKNER and BEELER, 2003) and as a function of effective stress (ZIMMERMAN, 1991). Furthermore, an additional content of clay particles inside the pore spaces has also been shown to cause the Skempton coefficient to decrease (AL-WARDY and ZIMMERMAN, 2004). The stiffening of the framework can be explained by closure of open micro-cracks at high confining pressure levels (MESRI et al., 1976).

The investigation of the mechanism, which leads to a change of permeability, porosity and Skempton coefficient depending on effective pressure is beyond the focus of the present study.

The aim of this paper is to show the impact of porosity, permeability and Skempton coefficient changes on the geothermal power production. For this purpose, relative changes of these parameters depending on the expected effective pressure change in our reservoir were measured by laboratory experiments and estimated by the mentioned relations. By means of the relative changes we get evidence about the hydraulic behavior of the rockmatrix during production and injection.

Laboratory Experiments

For our laboratory experiments three similar cylindrical shaped samples of Flechtinger sandstone were prepared. All samples were taken from one sandstone block with a dimension of 10cm x 10cm x 30cm. By means of these samples we tested permeability, porosity and Skempton coefficient under in situ conditions. A detailed description of these three experiments can be found in the following. In addition, mercury porosimetry was performed after the experiments on broken parts of the samples having a volume of approximately 1 to 2 cm^3. This independent method also yields a pore radius distribution of the samples as a function of the (effective) cumulative porosity as well as an average pore radius. In addition, the specific inner surface distribution is calculated from the mercury injection curve.

Permeability Measurement

The permeability experiment was performed in a High-Pressure-Temperature (HTP) permeameter (Figure 1), that allows a variety of continuous petrophysical measurements at a maximum temperature, lithostatic and pore pressure of 200°C, 140 MPa and 50 MPa, respectively. A detailed description of this apparatus can be found in MILSCH et al. (2007).

For investigating the permeability dependence on changes in effective pressure, a sample of Flechtinger sandstone was taken. The sample was cylindrical in shape with a diameter of 3 cm and a length of 4 cm. The permeability experiment was performed at a constant temperature of 40°C. A 0.1 molar NaCl-brine was used as the pore fluid which allowed a concurrent measurement of the electrical conductivity. The results of these measurements will be published elsewhere (MILSCH et al., 2008).

The experiment with the Flechtinger sandstone was performed at a maximum confining- and pore pressure of 47 MPa and 42 MPa, respectively. A constant flow rate of 0.05 $\frac{ml}{min}$ was applied.

We adjusted the effective pressure by increasing the confining pressure to its maximum and subsequently increased the pore pressure. Then, the pore pressure and the confining pressure were successively reduced to 2.5 MPa and 5 MPa, respectively. The increment of both pressures varied between 0.5 and 12.8 MPa. The described pressure cycling was repeated three times. During the experiment the pressure difference dp across the sample was measured. In order to keep the error (offset and/or drift of pressure sensors) in determining permeability as small as possible, a special measurement technique that refers to only one pressure sensor was applied. For this purpose, at each pressure step a bypass between the up- and the downstream side of the sample was opened and a reference value at the upstream side was measured. After closing the bypass the upstream pressure increased to a steady state value. Consequently, the pressure gradient ∇p can be calculated by the measured pressure difference and the length l of the sample. By means of the determined pressure gradient the permeability k of a rock is determined by a steady state method using Darcy's Law, thus assuming laminar flow conditions:

$$k = -\frac{Q * \eta}{A * \nabla p}, \tag{1}$$

where Q, A and η denote flow rate, the cross section of the sample and the dynamic viscosity of the fluid.

The permeability of the Flechtinger sandstone measured with the permeameter is shown in Figure 2. There, two issues were observed: An initial decrease in permeability for the first three pressure ramps (not shown here) and a decrease in permeability due to an effective pressure increase. The former is interpreted to be due to a consolidation of the non pre-conditioned sample. This consolidation is irreversible and leads to a steady deformation. After the consolidation process the rock acts completely linear elastic. Therefore, the decrease in permeability due to an increase in effective pressure can be assumed as poroelastic response. The determined permeability is $5.5 * 10^{-17} m^2$ at 3 MPa effective pressure and decreased to $4.3 * 10^{-17} m^2$ at 30 MPa effective pressure.

For a better illustration of the permeability decrease due to effective pressure increase, we also calculated the effective pressure derivative of permeability (fig. 2). The absolute permeability change decreased strongly from $-1.4 * 10^{-18} m^2/MPa$ to $-4.2 * 10^{-19} m^2/MPa$ at low effective pressure (p_{eff} = 4 to 10 MPa). Subsequently, the permeability change decreased to a minimum value of $-2.0 * 10^{-19} m^2/MPa$ at 21 MPa effective pressure and then it kept near con-

stant at effective pressure above 21 MPa. The constant value of permeability change indicates a linear decrease of permeability due to effective pressure change.

Porosity Measurement

The porosity measurement was performed at the same High-Pressure-Temperature (HTP) permeameter as in the permeability test. Therefore, the sample was cylindrical in shape with a diameter of 3 cm and a length of 4 cm. The temperature was kept constant at 40℃ and a 0.1 molar NaCl-brine was used as the pore fluid which allowed a concurrent measurement of the electrical conductivity. The experiment was carried out under hydrostatic conditions, so that the sample reacts to confining pressure only. During the first pressure ramp, the confining pressure was increased to a maximum of 50 MPa and was then reduced to the initial condition of 10 MPa. Subsequently, two further pressure cycles were performed with maximum confining pressure of 70 MPa. The confining pressure was controlled by adjusting the flowrate of the pressuring oil. For the porosity measurements we ensured an average confining pressure change of 0.13 $\frac{MPa}{min}$. During the total time of the experiment, the pore pressure p_p was kept constant at 5 MPa. Therefore, the effective pressure $p_{eff} = p_c - p_p$ ranged from 5 to 65 MPa. A direct measurement of porosity change depending on effective pressure change was impossible. Therefore, we determined the initial porosity at atmospheric pressure by means of mercury injection, 2D image analysis and weighting method. For our particular sample the initial porosity ϕ_{init} of 8.54% was determined by the ratio between fluid- and bulk volume. The fluid volume $V_f = 2.415g/1\frac{g}{cm^3}$ can be obtained by the dry and wet sample mass, which were 67.715 g and 70.130 g. The bulk volume $V_b = 28.27cm^3$ can be calculated by means of the sample dimensions. During the total time of the experiment, we measured the required fluid volume dV which was removed and added to the sample to ensure a constant pore pressure of 5 MPa. This fluid volume is defined negative because it indicates a loss of pore volume. By means of the initial fluid volume V_f, the sample volume V_b and the removed amount of water dV, the porosity ϕ can be calculated as follows:

$$\phi(dV) = \frac{V_f + dV}{V_b}. \tag{2}$$

The calculated porosity of the three confining pressure ramps are shown in Figure 3. It is obvious, that during the first and the beginning of the second confining pressure ramp an irreversible porosity loss occurred. In contrast, the second part of second pressure cycle as

well as the complete third pressure cycle show the linear-elastic behavior of the Flechtinger sandstone. This linear-elastic behavior leads to a decrease in porosity due to an increase of effective pressure. The determined porosity is 0.076 at 6 MPa effective pressure and decreased to 0.068 at 65 MPa effective pressure.

As for the permeability measurement, we also calculated the effective pressure derivative of porosity (fig. 3). There, the strongest reduction of porosity change from $3.2 * 10^{-4}$ 1/MPa to $1.5 * 10^{-4}$ 1/MPa was observed in a range between 7 MPa and 20 MPa effective pressure. A further reduction of porosity change to $7.0 * 10^{-5}$ 1/MPa at 51 MPa effective pressure followed and for higher effective pressure the porosity change was constant. This indicates a linear decrease of porosity due to effective pressure.

Skempton Coefficient Measurement

For the Skempton coefficient measurement, a sample of Flechtinger sandstone identical to the permeability and porosity experiments before was examined. At the pre-experimental stage, the sandstone samples were completely saturated within the hydraulic system. The samples underwent a two day flow-trough with distilled water before the pore pressure ports of the hydraulic system were closed to ensure a maximum saturation of more than 95%. The saturation was measured following the procedure of SMITH and SMITH (1998).

The sample was cylinder shaped with a diameter of 5 cm, a length of 10 cm and a porosity of ca. 8.3% was determined. The total volume of the sandstone cylinder was 196.4 cm^3 and the pore volume was ca. 16.3 cm^3. For measuring the axial and lateral strains of the sandstone samples, two axial extensometers and one radial chain extensometer were installed (MTS, 2004). The sample was mounted inside the pressure chamber (Fig. 4). This test system allows confining pressure up to 140 MPa. To apply hydrostatic conditions, the chamber was filled with a pressuring oil, and to keep the sample from being contaminated, it was surrounded by a silicon jacket. The mechanical system as well as the hydraulic system was connected to the Flechtinger sandstone. To minimize the dead volume of the hydraulic system, all capillaries were plugged by wires and the remaining dead volume was measured to 4 ml; this is equivalent to 25% of pore volume. This additional volume in the tubing exterior can significantly influence measurements of B (GREEN and WANG, 1986). WISSA (1969) suggested to minimize the ratio of exterior saturant volume to sample pore volume (0.3%), because the exterior saturant volume acts as a pore fluid reservoir and violates the undrained condition $dm_f = 0$. Therefore,

it can be assumed that the measured values of B are significant lower than for fully undrained condition. Hence, our measurements specify a lower boundary.

To reduce the irreversible deformation and to minimize the non-linear effects, we preconditioned the Flechtinger sandstone sample by applying a pressure cycle from 5 to 50 MPa, and repeated this procedure three times (according to HART and WANG, 1995). The raising of the confining pressure from 5 to 50 MPa and its lowering was done in 15 min. Throughout the preconditioning, the pore system was open to the atmosphere to achieve drained conditions.

In the first part of the Skempton experiment we measured the undrained poroelastic properties of an intact (without visible damage) Flechtinger sandstone at confining pressures from 5 to 50 MPa. The experiment was carried out at hydrostatic conditions so that sample properties are related to changes in confining pressure p_c. To show the reversibility of the induced pore pressure change the confining pressure was increased to a maximum of 50 MPa and was then reduced to the initial conditions five times. We measured the elastic deformation of the sandstone given by its axial and radial extension, as well as the pore pressure throughout the experiment. By means of the measured pore pressure change we determined the isotropic Skempton coefficient defined by $B = \frac{dp_p}{dp_c}$ (LOCKNER and BEELER, 2003). After closing the shut-off valves of the hydraulic system, the confining pressure was increased at a constant rate of 0.075 $\frac{MPa}{min}$ to its highest level of 50 MPa. At this level, the confining pressure was kept constant for 4 hours and was then decreased to its initial condition, again at a constant rate of 0.075 $\frac{MPa}{min}$. At the beginning of the first pressure cycle, the isotropic Skempton coefficient increased with increasing effective pressure to 20 MPa. This could be due to a possible dissolution of gas in the fluid of an incompletely saturated sample. Therefore, an additional saturation of the sample was performed. By means of the described ramps an effective pressure range $p_{eff} = p_c - p_p$ of approximately 10 MPa was applied. Therefore, two additional cycles were performed, where the confining pressure was increased to a maximum of 95 MPa and subsequently reduced to 5 MPa, resulting in an effective pressure range from 4 to 26 MPa. These two cycles started with the adjustment of the initial conditions, which were 5 MPa for confining pressure and 2.8 MPa for pore pressure. After closing the shut-off valves the confining pressure was increased at constant steps of 10 MPa to its highest level of 95 MPa. At this level, the confining pressure was kept constant for 1h and was then decreased to its initial condition, again at constant steps of 10 MPa. During the two additional pressure cycles the Skempton coefficient decreased with increasing effective pressure from 0.81 at 4 MPa to a minimum of 0.62 at 25 MPa.

There are two limiting boundaries for the isotropic Skempton coefficient: if the confining pressure affects only the grain structure it should be zero, and if the confining pressure affects only the fluid inside the pore spaces it should be one. We assume that the decrease of the Skempton coefficient results from the changing ratio of pore volume to grain volume as well as from a change of the pore-space geometry. This leads to a higher bulk modulus of the sample. On the one hand, the water is more compressible than the grains, therefore the pore volume decreases with increasing effective pressure. On the other hand, irregular pore spaces were more sensitive to effective pressure, therefore their shapes became more pressure resistent, and pore throats and micro-cracks were closed. This geometry change caused by closing of micro-cracks and elastic deformation of grains resulted in a more stable structure.

To investigate the dependence of the Skempton coefficient on effective pressure change, we differentiated the isotropic Skempton coefficient with respect to effective pressure (Fig. 5). The derivatives of these equation shows that the change of the Skempton coefficient was highest at low pressure and was reduced by an increasing effective pressure. The initial value of Skempton coefficient change was $1.3 * 10^{-2}$ 1/MPa at $p_{eff} = 5MPa$ and decreased to $7.3 * 10^{-3}$ 1/MPa at $p_{eff} = 15MPa$. For higher effective pressure, the Skempton coefficient change was near constant at $6.6 * 10^{-3}$ 1/MPa.

Estimation of Permeability and Skempton coefficient at Reservoir Condition

As mentioned in the introduction, for the geothermal power production in Gross Schönebeck an effective pressure range of $42.9 \pm 10MPa$ can be assumed. Only the porosity measurement included this effective pressure range and the determined values are listed in Table 1. The permeability and Skempton coefficient measurements were conducted to effective pressure values of 30 MPa and 25 MPa, respectively. Above these effective pressure levels both rock properties showed a near linear dependence on effective pressure. Therefore a linear approximation for higher effective pressure levels can be sufficient. The permeability change was determined with $-2.0 * 10^{-19} m^2/MPa$ and the change of Skempton coefficient was $-6.6 * 10^{-3}$ 1/MPa. By means of the permeability value at 30 MPa effective pressure ($4.3 * 10^{-17} m^2$) and the Skempton coefficient value at 25 MPa effective pressure (0.619) and its pressure dependence, values within the target effective pressure range can be linear extrapolated (Table 1). These derived values are

only rough estimations based on measurements below the target pressure range. Therefore, a better approximation of permeability and Skempton coefficient based on the measured porosity change should be derived in the following.

Permeability Calculation

The aim of this calculation is an extrapolation of permeability at high effective pressure by means of empirical model concepts. Various models exist, which correlate permeability and porosity based on pore space geometry attributes, such as hydraulic radius, inner surface, tortuosity, etc.. In order to derive permeability values at effective pressure between 33 MPa and 53 MPa, we tested three of these models: 1^{st} hydraulic radius model based on Kozeny-Carman-equation (KOZENY, 1927; CARMAN, 1937), 2^{nd} permeability-porosity relation of Rotliegend sandstones based on a fractal approach by PAPE et al. (2000) and 3^{rd} permeability calculation by mercury injection test based on percolation theory mentioned by KATZ and THOMPSON (1987).

For the first permeability calculation the equation $k = \frac{\phi * R^2}{6}$ was used, there R denotes the hydraulic radius. The hydraulic radius $R = \frac{\phi}{M}$, was determined by use of mercury injection method (there M is the specific inner surface). This model led to a permeability $k = 1.37 * 10^{-19} m^2$ at atmospheric pressure. For the second permeability calculation the equation $k = 155\phi + 37315\phi^2 + 630(10\phi)^{10}$ was used. This equation is based on a fractal model for Rotliegend sandstones of northeast Germany and was calibrated at several core sample measurements. It led to a permeability of $k = 2.07 * 10^{-16} m^2$ at atmospheric pressure. The third calculation based on the mercury injection led to a permeability of $k = 5.92 * 10^{-16} m^2$ at atmospheric pressure. For our specific rock sample a permeability of $k = 5.5 * 10^{-17} m^2$ was measured. In consideration of approx. 8% porosity, the permeability of our sample was lower than assumed. The model calculations by Pape and Katz & Thompson confirm this result. Therefore, we used the more general definition of permeability (BEAR, 1972):

$$k = f(s) * f(\phi) * L^2, \tag{3}$$

there $f(s)$, $f(\phi)$ and L^2 denote a function of shape, a function of porosity and a reference length square, respectively. The reference length can be the hydraulic radius or particle size as well. In order to find a linkage between permeability and porosity, the often used function of porosity $f(\phi) = \phi^3/(1-\phi)^2$ (BEAR, 1972) was chosen. There the porosity function can be directly

calculated by means of the laboratory results. The cross-plot of measured permeability and porosity function (fig. 6) shows a near linear dependency of the permeability k on the porosity function $f(\phi)$. Therefore, a constant geometry term $f(s)L^2$ over the total range of effective pressure can be assumed. To verify this assumption, the geometry term was calculated over the total range of effective pressure by means of $f(s)L^2 = k/f(\phi)$, as shown in Figure 6. It becomes obvious, that the geometry term depends on effective pressure itself. Although the influence of the geometry term on permeability was small in comparison to the porosity function, we derived a linear dependency of the geometry term on effective pressure $f(s)L^2 = 0.1627p_{eff} + 98.348$. There the unit of $f(s)L^2$ is $[10^{-15}m^2]$ and thus of p_{eff} is [MPa].

By means of Equation (3) and the definitions of geometry term and porosity function, we were able to calculate the permeability at each point of effective pressure, where the porosity was known. The results of these calculation are shown in Figure 7 and Table 2. With these calculations the measured permeability values can be well reproduced and lead to a better prediction of permeability in the effective pressure range between 33 MPa and 53 MPa. Although, the new calculated values differs marginal in comparison to the linear extrapolation, the permeability values based on porosity and geometry seem more accurate. For an effective pressure range of $p_{eff} = 43MPa \pm 10MPa$, we calculated a permeability range of $k = 4.08 * 10^{-17}m^2 \pm 4.9\%$ with linear extrapolation and a maximum change of $k = 4.14 * 10^{-17}m^2 \pm 3.6\%$ based on porosity measurement.

Skempton Coefficient Calculation

In contrast to permeability, the isotropic Skempton coefficient can be expressed in terms of the bulk module (K) and the porosity ϕ (DETOURNAY and CHENG, 1993):

$$B = \frac{\frac{K_f}{\phi}\left(1 - \frac{K_{fr}}{K_s}\right)}{\frac{K_f}{\phi}\left(1 - \frac{K_{fr}}{K_s}\right) + K_{fr}\left(1 - \frac{K_f}{K_s}\right)}, \tag{4}$$

where the subscripts f, fr and s stand for fluid, framework and solid, respectively. By means of this equation we derived Skempton coefficient values in the target effective pressure range of $p_{eff} = 43MPa \pm 10MPa$. The first step was the calculation of Skempton coefficient based on the porosity measurements. Since porosity was measured at effective pressure change, Skempton coefficient depends on effective pressure as well (Figure 8). The results of this calculation were unsatisfying, because the porosity change showed no significant effect on Skempton coefficient.

It is a well known fact, that the Skempton coefficient strongly depends on the bulk modulus. Therefore, the bulk modulus of the fluid, the solid and the framework over the observed effective pressure range had to be determined. Values for the bulk modulus of the fluid considered as pure water could be taken from the program REFPROP (LEMMON et al., 2007). The main fraction of the mineral content of the Flechtinger sandstones is quartz. Therefore, the bulk modulus of quartz (LEVIEN et al., 1980) was taken for the solid. Due to the fact, that the bulk modulus of the framework was not determined by our laboratory experiments, we used published data as well (TIGREK et al., 2005).

As porosity, calculations have shown that also the bulk modulus of the fluid and of the solid have no significant effect on the Skempton coefficient. In contrast, the effective pressure dependent bulk modulus of the framework characterized the change in Skempton coefficient (fig. 8). Although the absolute value of calculated and measured Skempton coefficient differs, the change of the Skempton coefficient with effective pressure can be reproduced. It has to be taken into account, that the curve of the calculated Skempton coefficient shows a break at $p_{eff} = 29MPa$. This could be a special effect of the specific sample used by TIGREK et al. (2005) and cannot be clarified here, because it was not discussed in the paper. For effective pressure values above 29 MPa the decrease of the Skempton coefficient is lower than expected by linear extrapolation. For an effective pressure range of $p_{eff} = 43MPa \pm 10MPa$, we calculated a Skempton coefficient range of $B = 0.500 \pm 13.2\%$ with linear extrapolation and a maximum change of $B = 0.646 \pm 2.5\%$ based on porosity and bulk modulus of the framework (tab. 2). The linear extrapolation values indicates the maximum change of Skempton coefficient over the observed effective pressure range. Due to the used bulk modulus of the framework, we assume that Skempton coefficient change calculated by porosity and bulk modulus is underestimated. The true Skempton coefficient change should be between these two calculated ranges, we expect a relative change of Skempton coefficient similar to thus of porosity and permeability.

Conclusions

To show the impact of poroelastic response of sandstones on geothermal power production at the research site Gross Schönebeck, we measured the effective pressure dependency of permeability, porosity and Skempton coefficient of Flechtinger sandstone, an outcropping equivalent of our reservoir rock. For the future geothermal power production flow rates will be about $100m^3/h$,

resulting in an effective pressure change of $p_{eff} = 43MPa \pm 10MPa$ in the reservoir.

Only the porosity measurement included this effective pressure interval and maximum changes of $\phi = 0.0698 \pm 1.7\%$ were determined. By means of the porosity measurement and the permeability measurement a maximum permeability change of $k = 4.14 * 10^{-17} m^2 \pm 3.6\%$ at $p_{eff} = 43MPa \pm 10MPa$ can be calculated. With additional values of bulk module of the Flechtinger sandstone similar relative changes in Skempton coefficient can be derived.

During the laboratory experiments, the permeability decreased by 21%, the porosity decreased by 11% and the Skempton coefficient decreased by 24%. These significant changes occurred at low effective pressures until 15 to 20 MPa. For our in situ reservoir conditions a change of 10 MPa effective pressure will result in a change in permeability of less than 4% and in porosity of less than 2%. Besides the rock matrix, a geothermal system consists of natural fractures and fault zones as well as induced hydraulic fractures. The hydraulic properties of all these components can be assumed as effective pressure dependent. In addition, chemical reactions such as precipitation and dissolution can significantly influence the productivity of the reservoir. In contrast to the above mentioned facts, we can conclude that the determined poroelastic responses did not affect the sustainability of the geothermal reservoir.

References

AL-WARDY, W. and ZIMMERMAN, R. W. (2003). Effective stress law for the permeability of clay-rich sandstones. *16th ASCE Engineering Mechanics Conference*, July 16–18, University of Washington, Seattle.

AL-WARDY, W. and ZIMMERMAN, R. W. (2004). Skempton coefficient of clean and clay-rich sandstones. *In: Proceedings of 17th ASCE Engineering Mechanics Conference*, University of Delaware, Newark, DE, 6.

BEAR, J. (1972). Dynamics of fluids in porous media. *Elsevier*, 764 pp.

BERNABE, Y. (1987). The effective pressure law for permeability during pore pressure and confining pressure cycling of several crystalline rocks. *Journal of Geophysical Research*, 92, 649–657.

BERNABE, Y. (1988). Comparison of the effective pressure law for permeability and resistivity formation factor in chelmsford granite. *PAGEOPH*, 127, No. 4.

CARMAN, P. (1937). Fluid flow through granular beds. *Trans. Inst. Chem. Eng. London*, 15, 150.

CARROLL, M. and KATSUBE, N. (1983). The role of terzaghi effective stress in linear elastic deformation. *J. Energy Resour. Tech.*, 105, 509–511.

DETOURNAY, E. and CHENG, A. H. D. (1993). Fundamentals of poroelasticity, analysis and design methods. *Pergamon Press*, Chapter 5 in Comprehensive Rock Engineering: Principles, Practice and Projects, Vol. II, Analysis and Design Method, 113–171.

GREEN, H. G. and WANG, H. F. (1986). Fluid pressure response to undrained compression in saturated sedimentary rock. *Geophysics*, 51, 4, 948–956.

HART, D. J. and WANG, H. F. (1995). Laboratory measurements of a complete set of poroelastic moduli for berea sandstone and indiana limestone. *Journal of Geophysical Research, B, Solid Earth and Planets*, 100, 17741-17751.

KATZ, A. and THOMPSON, A. (1987). Prediction of rock electrical conductivity from mercury injection measurements. *Journal of Geophysical Research*, 92, 599–607.

KOZENY, J. (1927). Über die kapillare leitung des wassers im boden (aufstieg, versickerung und anwendung auf die bewässerung. *Sitz. Ber. Akad. Wiss. Wien. Math. Nat. (Abt. IIa)*, 136a, 271-306.

KWON, O., KRONENBERG, A., GANGI, A., and JOHNSON, B. (2001). Permeability of wilcox shale and its effective pressure law. *Journal of Geophysical Research*, 106, 19.339–19.353.

LEGARTH, B., HUENGES, E., and ZIMMERMANN, G. (2005). Hydraulic fracturing in a sedimentary geothermal reservoir: Results and implications. *International Journal of Rock Mechanics and Mining Sciences*, 42, 1028–1041.

LEMMON, E., HUBER, M., and McLINDEN, M. (2007). Reference fluid thermodynamic and transport properties-refprop, version 8.0. *National Institute of Standards and Technology, Gaithersburg*, NIST Standard Reference Database 23.

LEVIEN, L., PREWITT, C., and WEIDNER, D. (1980). Structure and elastic properties of quartz at pressure. *American Mineralogist*, 65, 920–930.

LOCKNER, D. A. and BEELER, N. M. (2003). Stress-induced anisotropic poroelasticity response in sandstone. *In: Proceedings of 16th ASCE Engineering Mechanics Conference*, University of Washington, Seattle, WA, July 16–18, 2003.

LOCKNER, D. A. and STANCHITS, S. A. (2002). Undrained poroelastic response of sandstones to deviatoric stress change. *Journal of Geophysical Research, B, Solid Earth and Planets*, 107, 30.

MESRI, G., ADACHI, K., and ULLRICH, C. R. (1976). Pore pressure response in rock to undrained change in all-round stress. *Géotechnique*, 25, 317-330.

MILSCH, H., BLÖCHER, M., and ENGELMANN, S. (2008). Coupling of hydraulic and electrical transport properties in sandstones: An experimental evaluation of several scaling models. *Earth and Planetary Science Letters*, in press.

MILSCH, H., SPANGENBERG, E., KULENKAMPFF, J., and MEYHÖFER, S. (2007). A new apparatus for long-term petrophysical investigations on geothermal reservoir rocks at simulated in-situ conditions. *Transp. Porous Med.*, doi 10.1007/s11242-007-9186-4.

MOECK, I., SCHANDELMEIER, H., and HOLL, H. G. (2008). The stress regime in a rotliegend reservoir of the northeast german basin. *International Journal of Earth Sciences*, in press.

MORROW, C., BO-CHONG, Z., and BYERLEE, J. (1986). Effective pressure law for permeability of westerly granite under cyclic loading. *Journal of Geophysical Research*, 91, 3870–3876.

MTS (2004). Mts rock and concrete mechanics testing systems. *MTS Systems Corporation, 14000 Technology Drive Eden Prairie, MN USA 55344.*

PAPE, H., CLAUSER, C., and IFFLAND, J. (2000). Variation of permeability with porosity in sandstone diagenesis interpreted with a fractal pore space model. *Pure appl. geophys*, 157, 603-619.

SHAPIRO, S. A. (2003). Elastic piezosensitivity of porous and fractured rocks. *Geophysics*, 68, 2, 482–486.

SKEMPTON, A. W. (1954). The pore pressure coefficient a and b. *Géotechnique*, 4, 143-147.

SMITH, I. and SMITH, G. N. (1998). Elements of soil mechanics. *Blackwell*, Oxford.

TERZAGHI, K. (1923). Die berechnung der durchlassigkeitsziffer des tones aus dem verlauf der hydrodynamischen spannungserscheinungen. *Sitzungsberichte der Akadamie der Wissenchaften in Wien, Mathematisch-Naturwissenschaftliche Klasse, Abteihing, IIa*, 132, 105-124.

TIGREK, S., SLOB, E., DILLEN, M., CLOETINGH, S., and FOKKEMA, J. (2005). Linking dynamic elastic parameters to static state of stress: toward an integrated approach to subsurface stress analysis. *Tectonophysics*, 397, 167–179.

TRAUTWEIN, U. and HUENGES, E. (2005). Poroelastic behaviour of physical properties in rotliegend sandstones under uniaxial strain. *International Journal of Rock Mechanics and Mining Sciences*, 42, 7–8, 924–932.

WISSA, A. E. Z. (1969). Pore pressure measurement in satureted stiff soils. *J. Soil. Mech.*, 95, 1063–1073.

ZIMMERMAN, R. W. (1991). *Compressibility of Sandstones (Developments in Petroleum Science).*, volume 29, 173 pages. Elsevier Publishing Company.

ZIMMERMANN, G. and REINICKE, A. (2008). Hydraulic fracture stimulation of a deep sandstone reservoir to create an enhanced geothermal system (egs) - laboratory testing and field experiments. *AAPG Bulletin*, submitted.

ZIMMERMANN, G., REINICKE, A., BRANDT, W., BLÖCHER, G., MILSCH, H., HOLL, H.-G., MOECK, I., SCHULTE, T., SAADAT, A., and HUENGES, E. (2008). Results of stimulation treatments at the geothermal research wells in gross schönebeck/germany. *PROCEEDINGS, Thirty-Third Workshop on Geothermal Reservoir Engineering*, Stanford University, Stanford, California, January 28–30, SGP-TR-185.

ZOBACK, M. and BYERLEE, J. (1975). Permeability and effective stress. *American Association of Petroleum Geologists*, Bulletin 59, 154–158.

Table 1: Variation of permeability (linear extrapolated), porosity (measured) and Skempton coefficient (linear extrapolated) in the target effective pressure range between 33 MPa and 53 MPa. The relative value refers to the parameter value determined at in situ conditions.

parameter	$p_{eff} = 33MPa$ (rel. change)	$p_{eff} = 43MPa$ (in situ)	$p_{eff} = 53MPa$ (rel. change)
permeability k $[10^{-17}m^2]$ (extrapolated)	4.28 (**+4.9%**)	**4.08**	3.88 (**-4.9%**)
porosity ϕ	0.0710 (**+1.7%**)	**0.0698**	0.0688 (**-1.4%**)
Skempton coefficient B	0.566 (**+13.2%**)	**0.500**	0.434 (**-13.2%**)

Table 2: Variation of permeability (porosity dependent), porosity (measured) and Skempton coefficient (bulk module dependent) in the target effective pressure range between 33 MPa and 53 MPa. The relative value refers to the parameter value determined at in situ conditions.

parameter	$p_{eff} = 33MPa$ (rel. change)	$p_{eff} = 43MPa$ (in situ)	$p_{eff} = 53MPa$ (rel. change)
permeability k $[10^{-17}m^2]$	4.29 (**+3.6%**)	**4.14**	4.03 (**-2.7%**)
porosity ϕ	0.0710 (**+1.7%**)	**0.0698**	0.0688 (**-1.4%**)
Skempton coefficient B	0.653 (**+1.1%**)	**0.646**	0.630 (**-2.5%**)

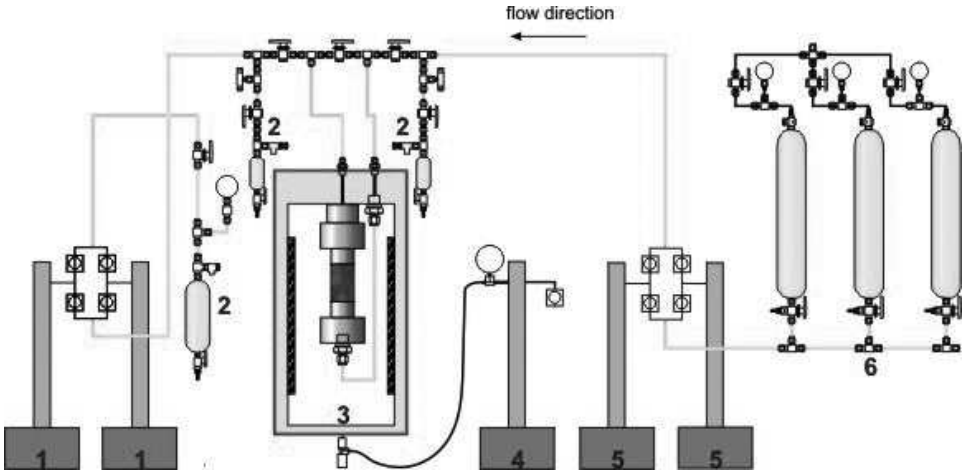

Figure 1: Schematic setup of the HTP-permeameter used for the permeability measurements: (1) downstream pump system maintains constant pore pressure (max. 50 MPa), (2) reservoirs for fluid sampling (max. 10 MPa), (3) pressure vessel with heater (max. 140 MPa and 200°C), (4) confining pressure pump (max. 140 MPa), (5) upstream pump system delivers constant fluid flow (max. 100 $\frac{ml}{min}$, max. 50 MPa) and (6) fluid reservoirs (10 l, max. 10 MPa)

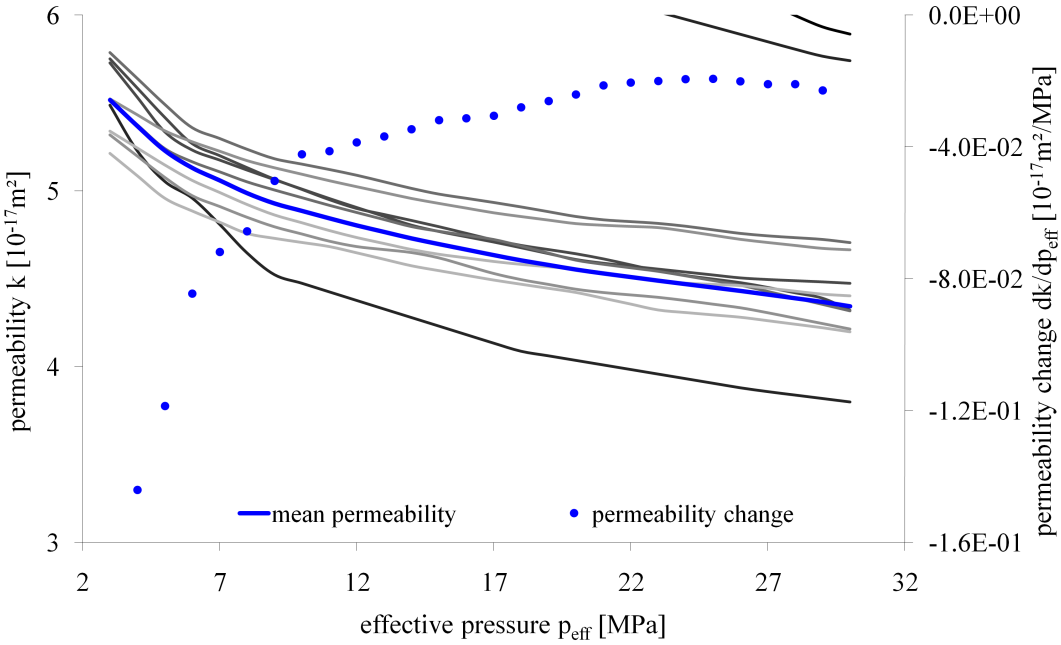

Figure 2: Permeability k measured for Flechtinger sandstone as a function of effective pressure. For each ramp we calculated the average permeability over an effective pressure interval of 1 MPa and subsequently the mean of the last nine pressure ramps. The color from black to light grey indicates the chronological sequence of the experiment. The dots indicate the permeability change over an effective pressure interval of 1 MPa.

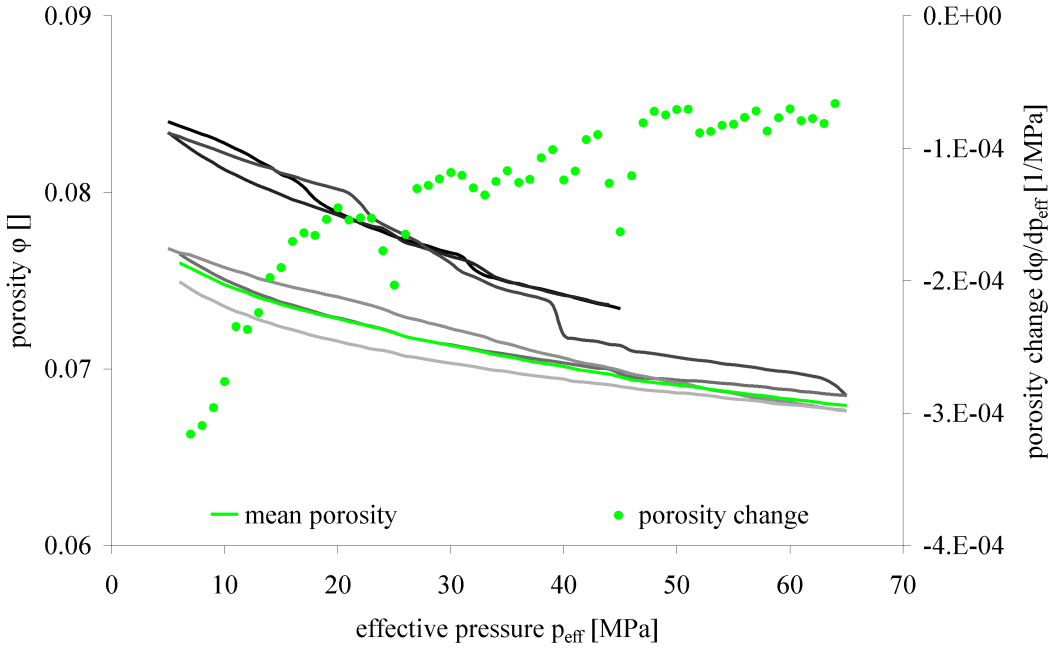

Figure 3: Porosity ϕ measured for Flechtinger sandstone as a function of effective pressure. For each ramp we calculated the average porosity over an effective pressure interval of 1 MPa and subsequently the mean of the last three confining pressure ramps. The color from black to light grey indicates the chronological sequence of the experiment. The dots indicate the porosity change over an effective pressure interval of 1 MPa.

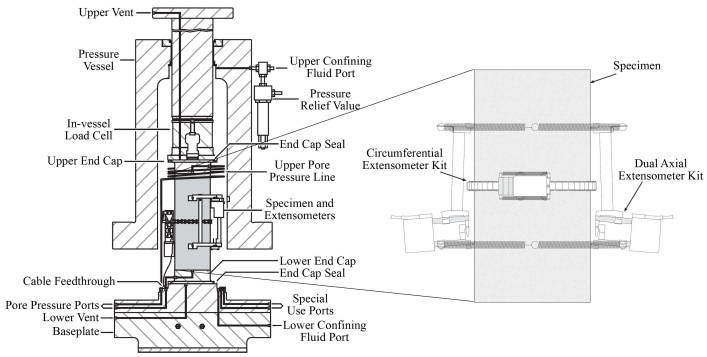

Figure 4: Laboratory test configuration showing Flechtinger sandstone sample in the pressure chamber (MTS, 2004). Pore pressure change was measured with the hydraulic shut-off valves closed to minimize external pore pressure system volume.

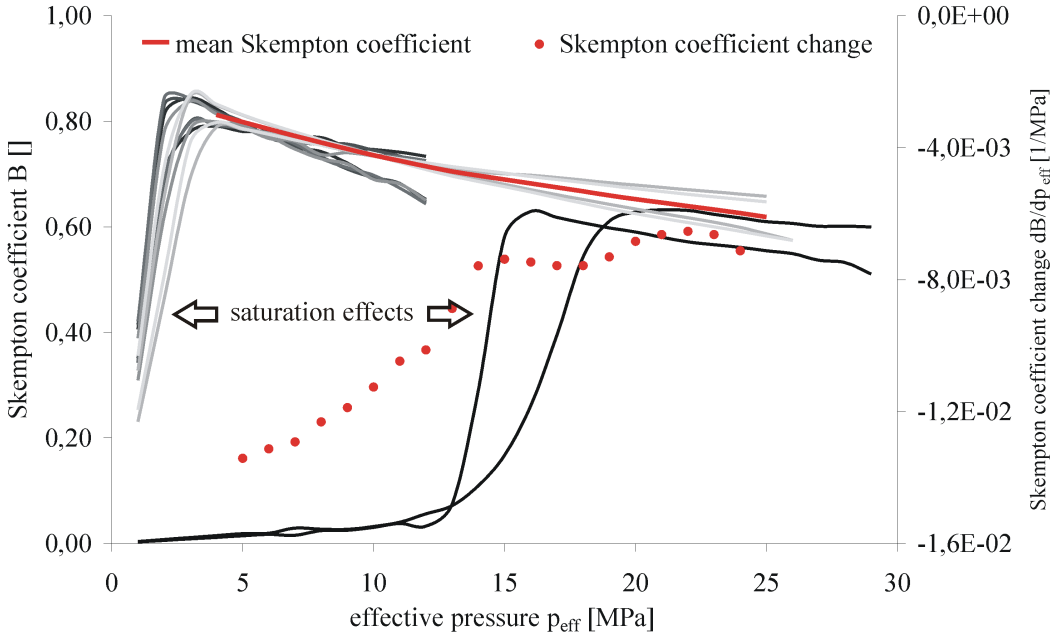

Figure 5: Skempton coefficient B measured for Flechtinger sandstone as a function of effective pressure. For each ramp we calculated the average Skempton coefficient over an effective pressure interval of 1 MPa and subsequently the mean of the last four confining pressure ramps. The color from black to light grey indicates the chronological sequence of the experiment. The vertical branches of the curves are due to a saturation deficit. The dots indicate the Skempton coefficient change over an effective pressure interval of 1 MPa.

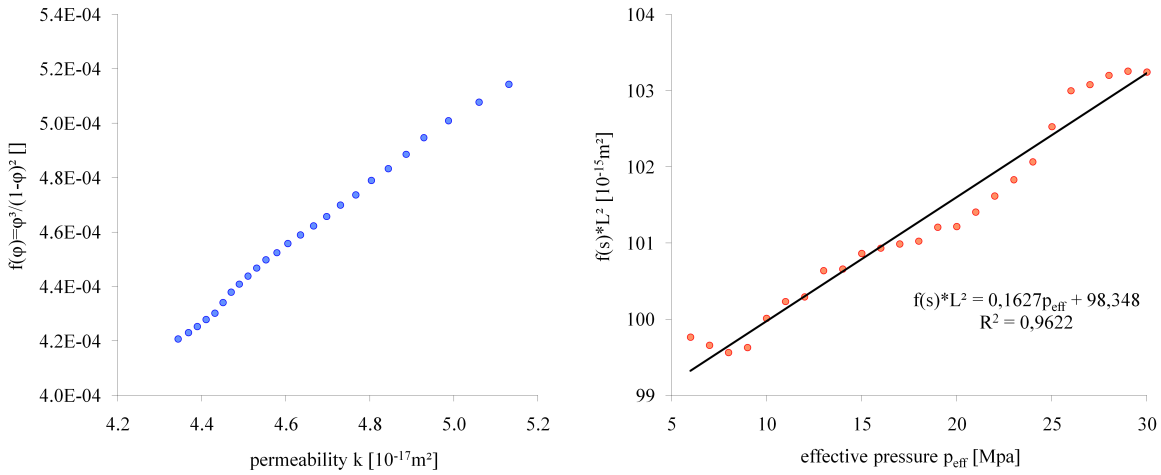

Figure 6: Cross-plot of measured permeability k and porosity function $\phi^3/(1-\phi)^2$ (calculated by porosity measurements) (left) and geometry function $f(s)L^2$ depending on effective pressure (right).

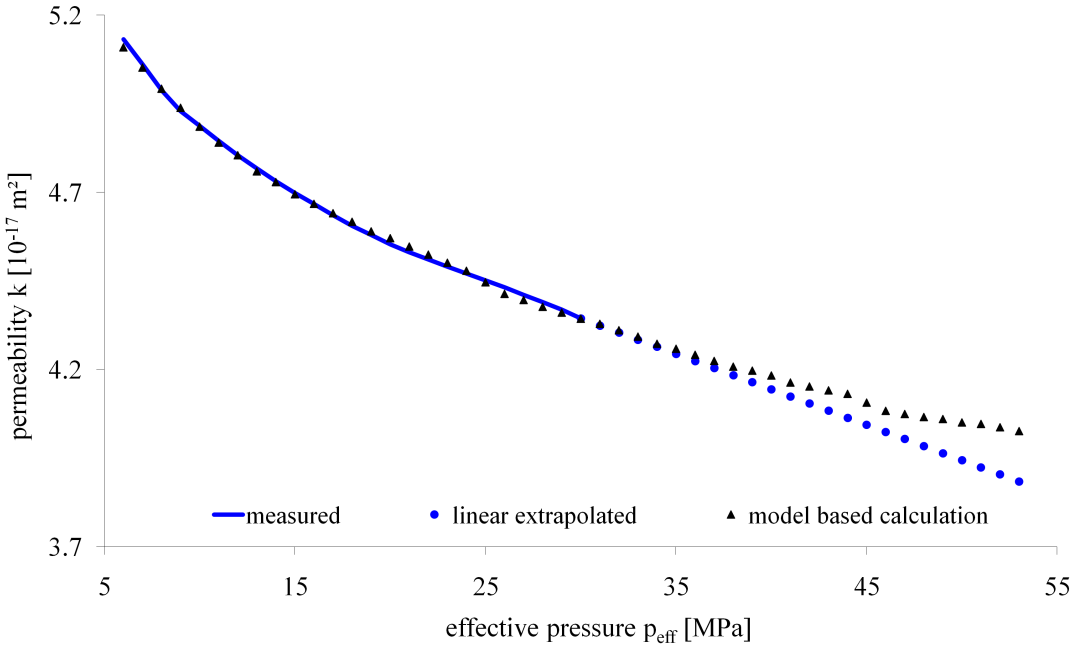

Figure 7: Permeability depending on effective pressure; measured by laboratory experiment (blue curve), extrapolated (blue dots) and calculated by means of porosity measurement (black triangles).

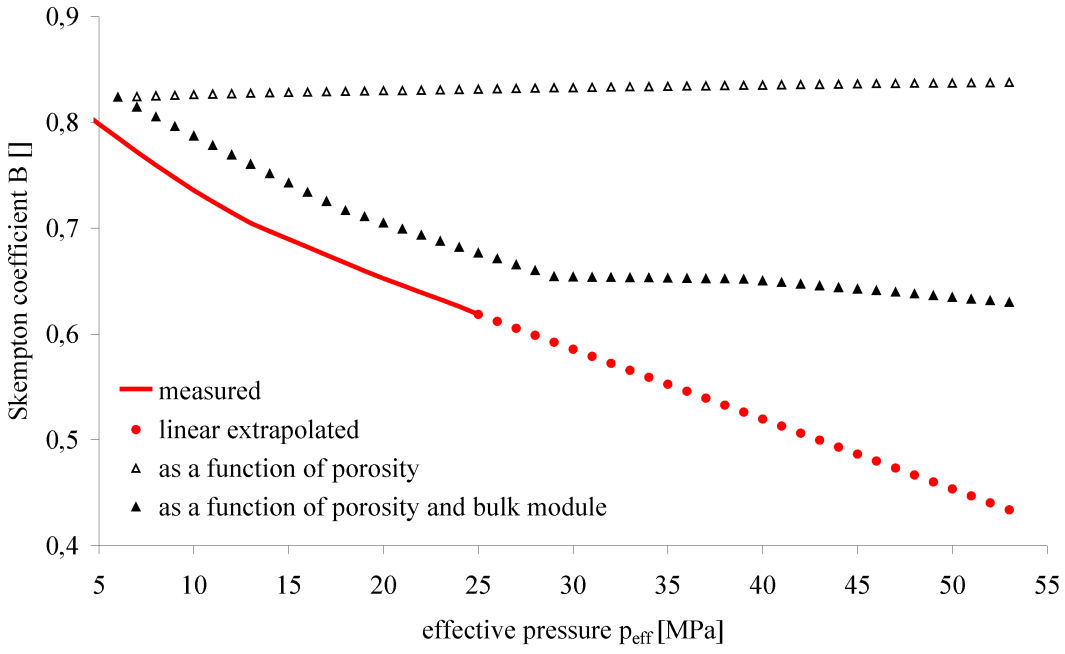

Figure 8: Skempton coefficient depending on effective pressure; measured by laboratory experiments (red curve), extrapolated (red dots), calculated by means of porosity (white triangles) and calculated by means of porosity and bulk module (black triangles).